

Quiescent deformation of the Aniakchak Caldera, Alaska, mapped by InSAR

Oh-Ig Kwoun* } Science Applications International Corporation (SAIC), U.S. Geological Survey (USGS) Center for Earth
Zhong Lu* } Resources Observation and Science (EROS), Sioux Falls, South Dakota 57198, USA
Christina Neal* U.S. Geological Survey, Alaska Volcano Observatory, Anchorage, Alaska 99508, USA
Charles Wicks Jr.* U.S. Geological Survey, Earthquake and Volcano Hazards Program, Menlo Park, California 94025, USA

ABSTRACT

The 10-km-wide caldera of the historically active Aniakchak volcano, Alaska, subsides ~13 mm/yr, based on data from 19 European Remote Sensing Satellite (ERS-1 and ERS-2) interferometric synthetic aperture radar (InSAR) images from 1992 through 2002. The pattern of subsidence does not reflect the distribution of pyroclastic deposits from the last eruption in 1931 and therefore is not related to compaction of fragmental debris. Weighted least-squares inversion of the deformation maps indicates a relatively constant subsidence rate. Modeling the deformation with a Mogi point source locates the source of subsidence at ~4 km below the central caldera floor, which is consistent with the inferred depth of magma storage before the 1931 eruption. Magmatic CO₂ and He have been measured at a warm soda spring within the caldera, and several sub-boiling fumaroles persist elsewhere in the caldera. These observations suggest that recent subsidence can be explained by the cooling or degassing of a shallow magma body (~4 km deep), and/or the reduction of the pore-fluid pressure of a cooling hydrothermal system. Ongoing deformation of the volcano detected by InSAR, in combination with magmatic gas output from at least one warm spring, and infrequent low-level bursts of seismicity below the caldera, indicate that the volcanic system is still active and requires close attention for the timely detection of possible hazards.

Keywords: volcanic processes, deformation, SAR, interferometry.

INTRODUCTION

Aniakchak volcano (Alaska, United States), a voluminous Pleistocene-Holocene stratovolcano with a summit caldera ~10 km in diameter, is located 670 km southwest of Anchorage on the Alaska Peninsula (Fig. 1). The caldera was formed by catastrophic eruption and collapse ca. 3.5 ka during an eruption of more than 50 km³ of andesite-dacite pyroclastic debris (Neal et al., 2001). Eruptions since this caldera-forming event have produced numerous vents inside the caldera, including tuff cones and a 1-km-high cinder and spatter cone, Vent Mountain (Fig. 1). The eruption of Half Cone within Aniakchak ~400 yr ago produced 0.75–1.0 km³ of material in a volcanic explosivity index (VEI) 3 or 4 eruption (Neal et al., 2001; Browne et al., 2004). Aniakchak's most recent eruption occurred in 1931, the only reported eruption in the past 250 yr. The 1931 eruption (VEI 3) was explosive and produced both lava and tephra from a series of vents near the western caldera wall. Although the main source of the eruption was a crater ~1 km in diameter (Main Crater in Fig. 1), blocky dacite lava flows issued from Slag Heap, Doublet Crater, and Main Crater (Fig. 1). Tephra deposits as much as 40 m

thick are distributed mostly on the northwestern part of the caldera floor and were erupted primarily from Main Crater (Fig. 1) (Nicholson, 2003). Seismic monitoring of Aniakchak volcano, initiated in 1997 by Alaska Volcano Observatory, has revealed no significant signs

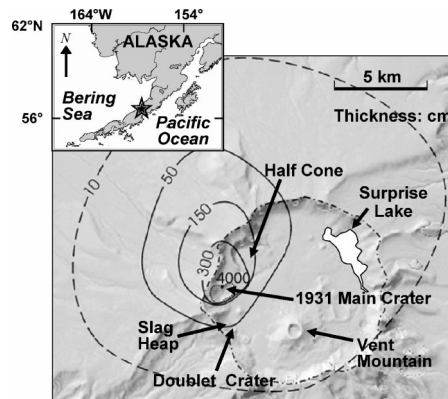


Figure 1. Aniakchak volcano, Alaska, a stratovolcano with circular summit caldera ~10 km in diameter, is located ~670 km southwest of Anchorage on the Alaska Peninsula. During 1931 eruption, lava was emitted from Main Crater, Slag Heap, and Doublet Crater. Solid lines indicate isopachs of tephra; dashed lines, uncertain thickness (Nicholson, 2003). This isopach map accounts for most lithic-rich tephra of 1931 eruption, constituting over 70% of total tephra volume.

of unrest, although occasional bursts of volcanic seismicity have been recorded (Jolly et al., 2001; Neal et al., 2001; Dixon et al., 2002, 2003, 2004).

Most volcanic processes are associated with measurable surface deformation patterns that can provide important insights into the structure, plumbing, and state of restless volcanoes (Dzurisin, 2003). Changes in the shape of a volcano can be precursory to an eruption; therefore, monitoring surface deformation of an active volcano is important even during quiescence (Lu et al., 2003a). The remote location of Aniakchak volcano and the harsh climate of the region result in expensive and complex logistics that hinder routine ground-based deformation surveys. Remote sensing techniques, especially spaceborne InSAR (interferometric synthetic aperture radar), provide a unique opportunity to cost-effectively monitor volcanic deformation under such circumstances (e.g., Lu et al., 2003b). Here, we applied an InSAR technique with satellite radar images to study deformation of Aniakchak volcano from 1992 through 2002.

DATA PROCESSING AND ANALYSIS

We use the two-pass InSAR approach (e.g., Massonnet and Feigl, 1998) to produce 19 deformation interferograms from 19 European Remote Sensing Satellite (ERS-1 and ERS-2) synthetic aperture radar (SAR) images, with interferometric baselines ranging from 12 to 282 m (Data Repository Figure DR1; Table DR1¹). The SAR data were collected during subarctic summers and autumns to avoid loss of coherence due to snow and ice accumulation. The 19 SAR images are from two different descending passes with center incidence angles of 21.3° and 23.5°, respectively. The corresponding line-of-sight (LOS) vectors (defined as east, north, up) are 0.353, -0.087, 0.932 and 0.387, -0.095, 0.917 for interferograms from these two passes. The digital elevation model (DEM) used to produce the de-

¹GSA Data Repository item 2006002, Figure DR1 and Table DR1, SAR image acquisition dates and baseline information, are available online at www.geosociety.org/pubs/ft2006.htm, or on request from editing@geosociety.org or Documents Secretary, GSA, P.O. Box 9140, Boulder, CO 80301-9140, USA.

*E-mails: okwoun@usgs.gov; lu@usgs.gov; tneal@usgs.gov; cwicks@usgs.gov.

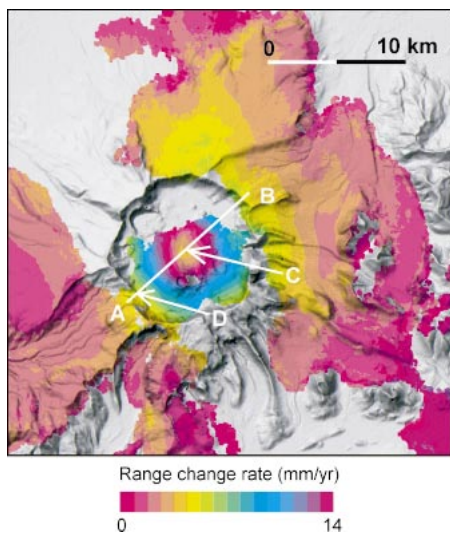


Figure 2. Stacked deformation interferogram of Aniakchak caldera showing mean subsidence rate from 1992 to 2002. Each fringe (full color cycle) represents 14 mm/yr of range change between ground and satellite in line-of-sight direction. Areas that lack interferometric coherence are uncolored.

formation interferograms is the 1-arc-second (~ 30 m posting) Shuttle Radar Topography Mission DEM, which has a relative vertical accuracy better than 10 m and an absolute vertical accuracy better than 16 m. DEM errors of this magnitude would result in no more than 5 mm of LOS range error in the interferograms (e.g., Massonnet and Feigl, 1998). The 19 interferograms indicate a continuing subsidence inside the 10-km-wide circular caldera, with the maximum subsidence near the center of the caldera floor.

The 19 interferograms are stacked in order to examine the mean deformation rate while reducing the effect of atmospheric delay anomalies. The phase values in the unwrapped interferograms are adjusted so that they are referenced to a common nondeforming point. Therefore, the preference is to use a nondeforming area outside the caldera. However, the steep topography along the caldera rim causes significant decorrelation along the rim, making phase unwrapping throughout the entire volcano very difficult. Therefore, we selected a reference point (D in Fig. 2 and in Figure DR2 [see footnote 1]) near the caldera rim, which is over an area least affected by the caldera deformation and which also can be unwrapped along with the coherent data points inside the caldera.

The radar incidence angles of the two adjacent ERS satellite tracks for these interferograms over the caldera center are different by less than 2° . This difference in radar incidence angles results in a difference in the measured deformation for interferograms over the same time interval; however, such a difference in range displacement along the LOS direction is

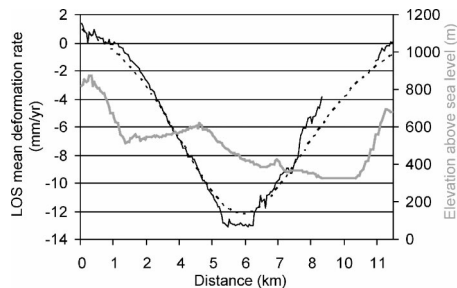


Figure 3. Mean deformation rate (black), modeled deformation rate by Mogi modeling (black dotted), and topographic profile (gray) along profile AB in Figure 2. Missing data in deformation profile are due to loss of coherence in associated interferograms. Observed subsidence exhibits no correlation with topography, excluding possibility of any strong topography related tropospheric artifacts. LOS—line of sight.

less than $\sim 5\%$ of the total range displacement. Therefore, we ignore the differences in LOS displacement implied by the difference in imaging geometry. The displacement maps from both tracks are stacked together to estimate a mean deformation rate along the LOS direction as follows:

$$\bar{\phi} = \frac{\sum_i \phi(i)}{\sum_i \Delta t(i)}, \quad (1)$$

where $\phi(i)$ is the deformation phase and $\Delta t(i)$ is the time span of the i th interferogram.

Figure 2 (also Figure DR2) is the stacked deformation interferogram, and Figure 3 is the mean deformation rate in the LOS direction along the profile AB in Figure 2. This profile indicates that the center of the caldera subsided ~ 13 mm/yr in the LOS direction from 1992 through 2002.

To further analyze the temporal evolution of the subsidence of the caldera floor, we apply a least-squares inversion, especially the linear minimum-norm deformation velocity model (Berardino et al., 2002), to the 19 interferograms that overlap in time. Although LOS deformation velocity may vary with time, the mean deformation between time-adjacent acquisitions is assumed constant. The phase variance estimated from each interferogram is used as a weight for the inversion. The relationship between the measured deformation map ($\Delta\phi$) and the unknown deformation phase velocity (v) is given as follows:

$$Bv = \Delta\phi \quad (2)$$

$$v^T = \left(\frac{\phi_1}{t_1 - t_0}, \dots, \frac{\phi_N - \phi_{N-1}}{t_N - t_{N-1}} \right) \quad (3)$$

$$\Delta\phi^T = (\delta\phi_1, \dots, \delta\phi_M) \quad (4)$$

$$v = (B^T W^{-1} B)^{-1} B^T W^{-1} \Delta\phi, \quad (5)$$

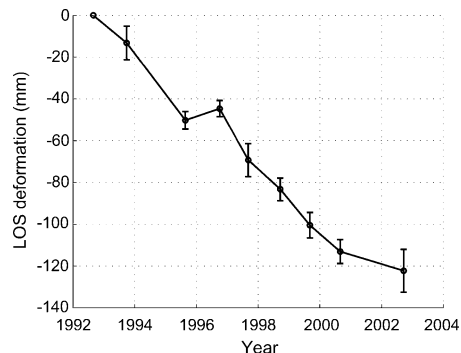


Figure 4. Maximum subsidence of caldera center (location C in Fig. 2) as function of time. Subsidence is relative to presumed nondeforming reference point (D in Fig. 2) near caldera rim. *F* test on deviations from mean velocity suggests that line-of-sight (LOS) deformation is linear with time at 90% confidence level. Deviation from mean during 2000–2002 might be due to possible atmospheric artifacts (only one interferogram spanning that interval was used in inversion).

where v is the unknown deformation velocity corresponding to each of the time-adjacent acquisitions, ϕ_j is the cumulative deformation phase at t_j with respect to t_0 , $\delta\phi_i$ is the deformation phase of interferogram i, B is an $M \times N$ matrix whose (i, j) element will be $B(i, j) = t_{k+1} - t_k$ within the time span covered by i th deformation phase ($\delta\phi_i$) or $B(i, j) = 0$ outside the time span, and W is an $M \times M$ diagonal matrix whose diagonal elements are phase variances of individual interferograms. Equation (2) is solved for v by applying the singular value decomposition to the matrix of equation (5) without temporal smoothing or adjustments of small singular values. The final solution ϕ_j is determined by an integration step, i.e.,

$$\phi_j = \sum_{k=1}^j v_k (t_k - t_{k-1}). \quad (6)$$

All SAR images were acquired between July and October to avoid interferometric decorrelation. As the deformation at Aniakchak is a slow process, we assume that the deformation rate from July through October in a single year is constant, and only invert the annual deformation rate. The interferograms are scaled according to their time durations before the inversion, and one deformation measurement point is given for each year (horizontal axis in Fig. 4). There were no suitable SAR images acquired in the years 1994 and 2001. Therefore, the inversion of 19 InSAR images results in only eight points in time (Fig. 4).

Figure 4 depicts a temporal evolution of deformation in the LOS direction in the region of maximum deformation of the caldera center, relative to the assumed stable reference point near the caldera rim (D in Fig. 2). Figure

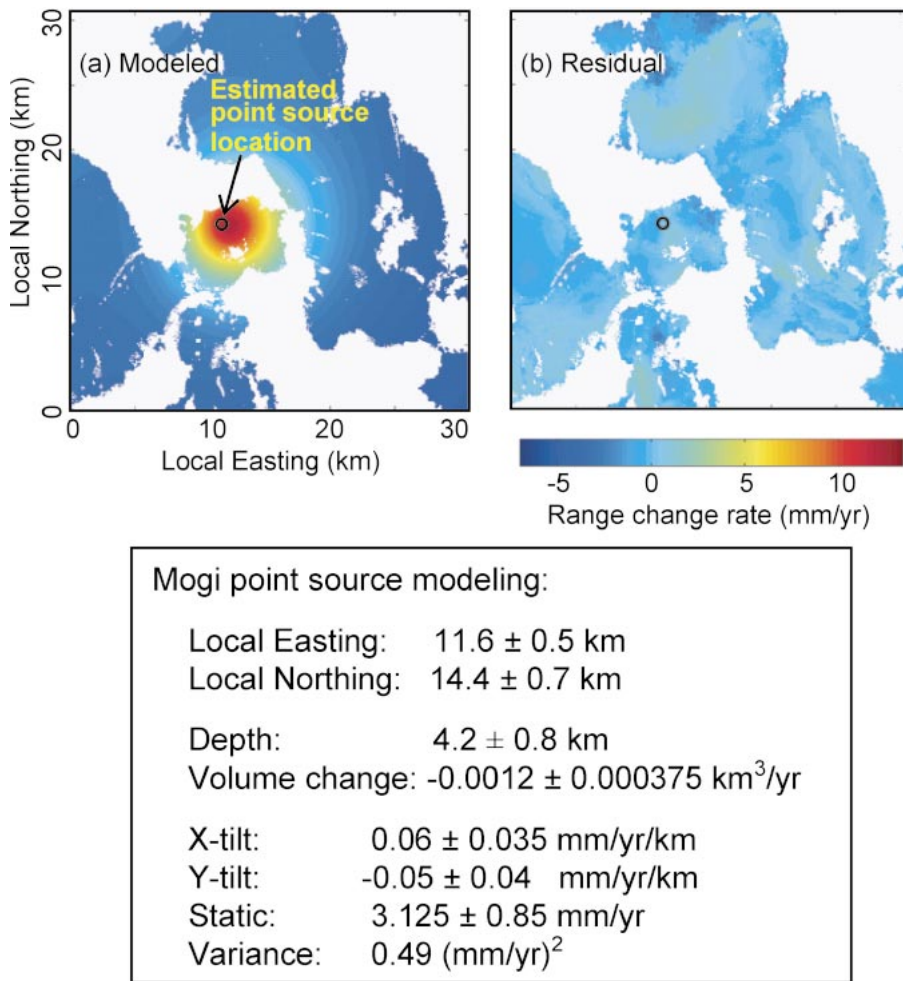


Figure 5. (A) Best-fit modeled and (B) residual interferograms of Aniakchak volcano, based on observed interferogram in Figure 2. Interferograms represent average deformation rate. Modeled interferogram was produced by using best-fit Mogi source at 4.2 km depth (black circle in A and B). Uncertainty bounds of Mogi parameters represent 95% confidence level. “Static” parameter is overall shift between calculated range change and observed range change, and is also inverted during deformation modeling. This parameter suggests that the reference, nondeforming point (point D) in Figure 2, moves at about -3 mm/yr. Areas lacking interferometric coherence are uncolored.

4 reveals a nearly constant LOS subsidence of the caldera from 1992 through 2002.

We modeled the average (annual) deformation image with a Mogi point source within homogenous elastic half-space (Mogi, 1958). The best-fit source is located at 4.2 km below the center of the caldera. The resulting volume change is -0.0012 km³/yr. The modeled interferogram and the residual interferogram (the difference between the observed and modeled interferograms) are shown in Figure 5 (also in Figure DR3 [see footnote 1]); and the profiles of the measured and modeled LOS mean deformation rates are compared in Figure 3. These indicate that the Mogi source fits the data remarkably well, with a variance of 0.49 (mm/yr)².

DISCUSSION AND IMPLICATIONS

The subsidence of large calderas is attributable to local or regional tectonic earthquakes, removal and migration of magmatic

or hydrothermal fluids, magma crystallization and thermal contraction and degassing, the depressurization of the hydrothermal reservoir, and/or a combination of all of the above (Newhall and Dzurisin, 1988; Mann and Freymueller, 2003). At Aniakchak volcano, no significant volcanic unrest has been observed or recorded since the last eruption in 1931. Seismic monitoring since 1997 indicates low rates of volcanic seismicity over the Aniakchak volcano region, and most volcano-tectonic earthquakes (all with magnitudes of less than 2) are centered at least 10 km away from the center of the caldera at depths of ~ 5 –10 km below sea level (Power et al., 2004). The hypocenters of deep long-period seismic events (with magnitudes less than 3) are located beneath the caldera (15–30 km deep), and some are scattered as much as 10 km away from the caldera, with depths of ~ 13 –28 km below sea level (Jolly et al., 2001; Dixon et al., 2002, 2003; Power et al., 2004). Therefore, we ex-

clude local earthquake activity as a cause for the observed caldera subsidence. However, it is intriguing that the subsidence has not induced much seismicity.

Was the observed subsidence at Aniakchak caldera caused by migration of magmatic or hydrothermal fluids? Within a 40 km radius from the center of the caldera, no substantial surface deformation outside the caldera is identifiable in the interferograms. It is possible that intrusion outside the caldera may have gone undetected or that atmospheric artifacts in interferograms could have obscured surface inflation signals related to the intrusion. However, there is no geological evidence of young volcanic vents outside the caldera, and constant migration of magma out of the caldera during the past decade is unlikely. Therefore, it is reasonable to exclude the possibility that the subsidence was caused by magma migration.

Inspection of individual interferograms of Aniakchak volcano indicates a near-concentric pattern of deformation over the caldera floor. The observed deformation is not due to the thermoelastic contraction of the pyroclastic deposits from the 1931 eruption because the patterns of subsidence do not appear to follow the distribution of the deposit (Fig. 1).

We offer the following preliminary model to explain this deformation pattern. Although the 1931 eruption occurred from a ring-fracture series of vents near the base of the west caldera wall (Fig. 1), the magma body that fed the 1931 eruption could have been located beneath the center of the caldera, as is commonly observed at other Aleutian volcanoes such as Okmok (Lu et al., 2000), Makushin (Lu et al., 2002), and Katmai (Hildreth, 1987). On the basis of water content and Fe-Ti oxide data, Bacon (2000) estimated that the pre-eruption magma storage depths for the last two significant eruptions at Aniakchak were 5 km for the 1931 event and 3 km for the 400 B.P. Half Cone eruption. Results from modeling the mean deformation interferogram indicate that the source of subsidence is ~ 4 km beneath the central caldera floor. The coincidence of depths, as assessed by petrologic analysis and modeling of a deformation source, suggests that the cause of the subsidence is related to cooling and crystallization of residual magma from recent eruptions, or magma intruded sometime between 1931 and 1992. The presence of a cooling magma body is consistent with ongoing discharge of magmatic CO₂ and He from a soda spring near Surprise Lake (Symonds et al., 2003). Hence, the observed subsidence also might be caused by the volume decrease of the active magma reservoir resulting from degassing.

In addition to the CO₂ soda spring, several fumaroles persist in pyroclastic deposits inside

the caldera (Miller et al., 1998; Neal et al., 2001). In 1973, temperatures of 80 °C were measured at a depth of 15 cm in coarse tephra ~1.5 km northeast of the Main Crater vent of the 1931 eruption. Additional sub-boiling point fumaroles are located at several spots on the north wall of Half Cone, the source of the 400 B.P. eruption (Fig. 1). The temperature of the springs near Surprise Lake was 25 °C in July 1993 and 24 °C in July 2002. Because these springs reflect circulation in an active hydrothermal system, the observed subsidence at Aniakchak caldera also might be caused by the reduction of pore-fluid pressure due to cooling of the system beneath the floor of the caldera.

CONCLUSIONS

InSAR images from different time intervals reveal that the central caldera of Aniakchak volcano has been subsiding at a rate of as much as 13 mm/yr. The deformation outside of the caldera is not substantial. The observed subsidence is most likely caused by cooling and degassing of a residual magma reservoir located ~4 km beneath the caldera center, and/or by the decreased pore-fluid pressure within a shallow hydrothermal system beneath the caldera. The depth of deformation source is consistent with that based on geochemical analysis (Bacon, 2000).

Understanding noncritical deformation at volcanoes (e.g., passive or background ground motion that is not cause for alarm) is important because ground deformation can reflect magmatic and other processes that presage an eruption, as well as those that are not precursory to an eruption. As instrumental monitoring of active volcanoes becomes more widespread, it is critical to differentiate between those deformation signals that are cause for concern and those that are not. This study suggests that subsidence at an active caldera system can be explained by posteruption processes, and not necessarily changes in the magmatic system related to an increased potential for eruption.

Despite low levels of background volcanic seismicity, Aniakchak's recent history of silicic explosive eruptions and the persistence of magmatic degassing indicate that the volcano is still active. As such, it is prudent to maintain systematic, multiparametric instrumental monitoring to establish background activity and to identify precursory changes that could lead to violent and hazardous eruptions. Aniakchak is located in a remote area with a harsh environment that makes ground-based leveling surveys or static GPS measurements difficult. This study shows that the spaceborne InSAR technique is a practical and effective

method for monitoring volcanic deformation in remote areas. Without InSAR remote sensing techniques, quiescent volcanic deformation processes at remote regions would likely go unnoticed (Lu et al., 2003b).

ACKNOWLEDGMENTS

ERS-1 and ERS-2 SAR images are copyrighted (1992–2002) by the European Space Agency (ESA) and were provided by the Alaska Satellite Facility (ASF). This research was supported by funding from NASA (NRA-99-OES-10 RADARSAT-0025-0056), U.S. Geological Survey (USGS) Volcano Hazards Program, USGS Land Remote Sensing Program, and USGS contract O3CRCN0001. We thank ASF for its excellent support in providing SAR data on a timely basis, John Power and Charles Bacon for many useful discussions on Aniakchak volcano, and Robert Nicholson for providing his thesis work.

REFERENCES CITED

- Bacon, C.R., 2000, Pre-eruptive volatiles in the most recent eruptions of Aniakchak Volcano, Alaska [abs.]: *Eos (Transactions, American Geophysical Union)*, v. 81, no. 48, p. 1376–1377.
- Berardino, P., Fornaro, G., Larnari, R., and Sansosti, E., 2002, A new algorithm for surface deformation monitoring based on small baseline differential SAR interferograms: *IEEE Transactions on Geoscience and Remote Sensing*, v. 40, p. 2375–2383, doi: 10.1109/TGRS.2002.803792.
- Browne, B.L., Neal, C.A., Gardner, C., and Eichelberger, J., 2004, A recent eruption at Aniakchak Caldera, Alaska: International Association of Volcanology and Chemistry of the Earth's Interior (IAVCEI) General Assembly, Pucon, Chile.
- Dixon, J.P., Stihler, S.D., Power, J.A., Tytgat, G., Estes, S., Moran, S.C., Paskievitch, J., and McNutt, S.R., 2002, Catalog of earthquake hypocenters at Alaskan volcanoes, January 1, 2000, through December 31, 2001: U.S. Geological Survey Open-File Report 02-342, 56 p.
- Dixon, J.P., Stihler, S.D., Power, J.A., Tytgat, G., Moran, S.C., Sanchez, J.J., Estes, S., McNutt, S.R., and Paskievitch, J., 2003, Catalog of earthquake hypocenters at Alaskan volcanoes, January 1 through December 31, 2002: U.S. Geological Survey Open-File Report 03-267, 58 p.
- Dixon, J.P., Stihler, S.D., Power, J.A., Tytgat, G., Moran, S.C., Sanchez, J.J., McNutt, S.R., Estes, S., and Paskievitch, J., 2004, Catalog of earthquake hypocenters at Alaskan volcanoes, January 1 through December 31, 2003: USGS Open-File Report 2004-1234, 69 p.
- Dzurisin, D., 2003, A comprehensive approach to monitoring volcano deformation as a window on eruption cycle: *Review of Geophysics*, v. 41, p. 1001, doi:10.1029/2001RG000107.
- Hildreth, W., 1987, New perspectives on the eruption of 1912 in the valley of Ten Thousand Smokes, Katmai National Park, Alaska: *Bulletin of Volcanology*, v. 49, p. 680–693, doi: 10.1007/BF01080359.
- Jolly, D., Stihler, S.D., Power, J.A., Lahr, J.C., Paskievitch, J., Tytgat, G., Estes, S., Lockheart, A.D., Moran, S.C., McNutt, S.R., and Hammond, W.R., 2001, Catalog of earthquake hypocenters at Alaskan volcanoes: January 1,

- 1994, through December 31, 1999: U.S. Geological Survey Open-File Report 01-189, 22 p.
- Lu, Z., Mann, D., Freymueller, J., and Meyer, D., 2000, Synthetic aperture radar interferometry of Okmok Volcano, Alaska: Radar observations: *Journal of Geophysical Research*, v. 105, p. 10791–10806, doi: 10.1029/2000JB900034.
- Lu, Z., Power, J., McConnell, V., Wicks, C., and Dzurisin, D., 2002, Pre-eruptive inflation and surface interferometric coherence characteristics revealed by satellite radar interferometry at Makushin Volcano, Alaska: 1993–2000: *Journal of Geophysical Research*, v. 107, no. B11, 2266, doi: 10.1029/2001JB000970.
- Lu, Z., Masterlark, T., Dzurisin, D., Rykhus, R., and Wicks, C., 2003a, Magma supply dynamics at Westdahl Volcano, Alaska, modeled from satellite radar interferometry: *Journal of Geophysical Research*, v. 108, no. B7, 2354, doi: 10.1029/2002JB002311.
- Lu, Z., Wicks, C., Dzurisin, D., Power, J., Thatcher, W., and Masterlark, T., 2003b, Interferometric synthetic aperture radar studies of Alaska volcanoes: *Earth Observation Magazine*, v. 12, no. 3, p. 8–18.
- Mann, D., and Freymueller, J., 2003, Volcanic and tectonic deformation on Unimak Island in the Aleutian Arc, Alaska: *Journal of Geophysical Research*, v. 108, no. B2, 2108, doi: 10.1029/2002JB001925.
- Massonnet, D., and Feigl, K., 1998, Radar interferometry and its application to changes in the Earth's surface: *Reviews of Geophysics*, v. 36, p. 441–500, doi: 10.1029/97RG03139.
- Miller, T.P., McGimsey, R. G., Richter, D. H., Riehle, J. R., Nye, C. J., Yount, M. E., and Dumoulin, J. A., 1998, Catalog of the historically active volcanoes of Alaska, United States, Alaska Volcano Observatory, Alaska: Geological Survey Open-File Report 98-582, 104 p.
- Mogi, K., 1958, Relations between the eruptions of various volcanoes and the deformations of the ground surface around them: *Bulletin of the Earthquake Research Institute, University of Tokyo*, v. 36, p. 99–134.
- Neal, C.A., McGimsey, R.G., Miller, T.P., Riehle, J.R., and Waythomas, C.F., 2001, Preliminary volcano-hazard assessment for Aniakchak Volcano, Alaska: U.S. Geological Survey Open-File Report 00-519, 35 p.
- Newhall, C.G., and Dzurisin, D., 1988, Historical unrest at large calderas of the world: U.S. Geological Survey Bulletin 1855, v. 1–2, 1108 p.
- Nicholson, R.S., 2003, The 1931 eruption of Aniakchak Volcano, Alaska: Deposit characteristics and eruption dynamics [M.S. thesis]: Fairbanks, University of Alaska Fairbanks, 270 p.
- Power, J.A., Stihler, S.D., White, R.A., and Moran, S.C., 2004, Observations of deep long-period (DLP) seismic events beneath Aleutian Arc Volcanoes; 1989–2002: *Journal of Volcanology and Geothermal Research*, v. 138, p. 243–266, doi: 10.1016/j.jvolgeores.2004.07.005.
- Symonds, R.B., Poreda, R.J., Evans, W.C., Janik, C.J., and Ritchie, B.E., 2003, Mantle and crustal sources of carbon, nitrogen, and noble gases in Cascade-Range and Aleutian-Arc volcanic gases: U.S. Geological Survey Open-File Report 03-436, 26 p.

Manuscript received 1 July 2005

Revised manuscript received 22 September 2005

Manuscript accepted 26 September 2005

Printed in USA